Electronic relaxation of Xe_2Cl in gaseous and supercritical fluid xenon

F. Okada[a] and V. A. Apkarian[b]
Department of Chemistry, University of California, Irvine, California 92717

(Received 28 July 1990; accepted 17 September 1990)

Spectroscopic and kinetic studies of the triatomic Xe_2Cl exciplex in gaseous and supercritical fluid xenon up to 150 atm are reported. Clustering of the exciplex with Xe atoms is observed and its effect on spectral shifts, radiative lifetimes, and collisional deactivation are discussed. A kinetic treatment, incorporating diffusion controlled encounter probabilities, is used for the analysis of the relaxation data throughout the studied range. The radiative lifetime of the exciplex is observed to be 328($\pm$20) ns, the exciplex is quenched by molecular chlorine with a rate constant of $7(\pm 1)\times 10^{-10}$ cm^3 s^{-1}, while quenching by Xe is imperceptible even at the highest densities, implying a rate constant $\leqslant 10^{-17}$ cm^3 s^{-1}. Observations of transient loss, and their implications with respect to condensed phase triatomic rare gas halide exciplex lasers, are discussed.

I. INTRODUCTION

The triatomic rare gas halides, $Rg_2^+X^-$, form a fascinating family of exciplexes that have been the subject of both theoretical and experimental studies in the gas phase.[1] More recently they have been employed in both solid state and liquid phase investigations of charge transfer and reaction dynamics.[2] Among the notable properties that makes these systems valuable probes in condensed phase investigations of structure, energetics, and dynamics are: (a) their unusual stability—in all cases the triatomic exciplexes are more stable than their diatomic (Rg^+X^-) counterparts by an energy equivalent to the binding energy of the diatomic rare gas ions (Rg_2^+), moreover they do not further react even in liquid or solid rare gases to form larger cluster ions, e.g., $Rg_3^+X^-$ (in recent gas phase studies,[3] convincing evidence has been presented for the presence of $Ar_3^+F^-$), (b) their very large dipoles—12.21 D in the case of $Xe_2^+Cl^-$ ($4\,^2\Gamma$)[4] —due to the nearly complete charge transfer in these ionic states, makes them sensitive probes of local structure; (c) their long radiative lifetimes,[5] characteristically between 100 and 300 ns, makes them amenable for studies with conventional laser sources; (d) finally, the fact that they can be very efficiently prepared by optical and electron beam pumping schemes in rare gas/halogen-donor mixes, makes them obvious candidates for both fundamental studies of charge transfer and reaction dynamics, and practical studies of condensed phase lasers.[1,2]

Historically, interest in the triatomic rare gas halide exciplexes evolved due to their suspected parasitic role in the operation of gas phase diatomic exciplex lasers. Laser action was subsequently demonstrated in both Xe_2Cl[6,7] and Kr_2F[8,9]by electron beam pumping of gas mixtures. However, due to their longer lifetimes, and broad bound-to-free emission profiles, stimulated emission cross sections of the triatomics are nearly two orders of magnitude smaller than their diatomic counterparts. As such, in order to achieve the necessary excited state number densities, such gas phase lasers by necessity can only be conceived at high pressures. An obvious alternative is to resort to condensed media. Indeed, very high densities of the triatomic exciplexes can be photogenerated in both solid and liquid rare gases.[2] Despite the fact that optically pumped laser operation of the diatomic XeF has been demonstrated in both the liquid[10] and solid phases,[11,12] laser action on the triatomics in similar media has not yet been reported. An understanding of the photodynamics of these systems at high densities is of obvious value for such considerations.

In this paper we report systematic studies of the relaxation dynamics of Xe_2Cl at room temperature and in high pressures of Xe—up to $\sim$150 atm. Relaxation studies have been previously conducted on the same system at low pressures.[6,13–17] The general conclusions from those studies were that while the deactivation rate of the exciplex by Cl_2 is nearly gas kinetic, its deactivation by Xe is very inefficient. Most investigators placed an estimated upper bound for the latter process—a rate of 6×10^{-15} cm^3 s^{-1} for deactivation by Xe was reported in an early study.[13] We have previously reported on relaxation studies of Xe_2Cl in liquid Xe.[18] There, it was found that in dilute solutions the deactivation of the exciplex was controlled by radiation. The direct observation of fluorescence decay rates of $\sim$200 ns in such solutions, places the deactivation rate by the solvent below 10^{-17} cm^3 s^{-1}. Those studies were however conducted in cryogenic liquids. Given the very large dipole of the exciplex and the large polarizability of Xe, many-body interactions could conceivably play a perceptible role in such media. For example, complexation of the exciplex with its solvent cage has been postulated to explain the absence of backreactions between Xe_2I and Cl in recent studies of ICl in liquid Xe.[19] Clustering in the liquid phase has also been postulated in order to explain the abrupt blue shift observed upon liquid–solid phase transitions.[20] Finally, the propensity of the polarizable cage to collapse around the exciplex has been advanced to explain the efficient charge transfer induced photodissociation of molecular halogens in solid rare gases,[2,5] and in particular for Cl_2 in solid Xe under high pressures.[21] The present studies were, therefore, designed to enable a di-

[a] Present address: Petroleum Division, Nippon Mining Co., LTD.; 10-1 Toranomon 2-Chome, Minato-Ku, Tokyo 105, Japan.
[b] Alfred P. Sloan Fellow.

 0021-9606/91/010133-12$03.00

rect comparison between relaxation dynamics in the different phases, with the anticipation of directly detecting the evolution of many-body control of dynamics. In addition to the relaxation measurements, emission spectra of the exciplex were recorded throughout the studied range of densities. Since this emission undergoes a large shift, it does provide an additional description of the interactions. Finally, and with the realization that the system kinetics were rather optimal for laser operation, several attempts were made for detection of gain in supercritical fluids. As will be described, instead of gain, a very strong attenuation of the injected probe beam was observed.

These results are presented in this paper, in Sec. III, after a brief exposition of the experimental methods (Sec. II). A discussion of the main findings and a kinetic model for the analysis of the rate processes throughout the studied range of pressures is provided in Sec. IV. A summary of the main conclusions is presented in Sec. V.

II. EXPERIMENTAL

The majority of the reported experimental studies were conducted in a four-window, high pressure cryocell. The cell body was constructed of OFHC copper to enable efficient cooling. The entire cell was electroplated with gold to minimize wall reactions with halogens. Sapphire windows of 1/8 in. thickness and 1/2 in. diameter were sealed on the cell with either an indium or Ca:Pb alloy. Neither of these gaskets was completely satisfactory due to their reactivities with halogens; however, the second choice proved more useful since the exposed areas could be minimized and therefore passivated. The cell was attached to an all monel manifold equipped with bellows valves with specified burst pressures of 700 psi, and vacuum service to better than 10^{-9} Torr. The manifold was equipped with a low pressure capacitance manometer (4.5 digit accuracy over the full range of either 1 or 10 Torr) for measuring the halogen pressure, and a 4 in. high pressure Bourdon gauge for measuring the Xe pressure (range 0–1000 psig, accuracy of 2.5 psi). The manifold-to-cell volume ratio was calibrated so that the Xe pressures in the cell could be measured by difference. To obtain supercritical densities, the entire cell is cooled by a dry-ice/methanol bath, the condensed sample is then returned to room temperature and allowed to equilibrate (typically for 1/2 h). The cell temperature was constantly monitored during the measurements and maintained at room temperature with a resistive heater. The Cl_2 sample, of manufacturer's specified purity of 99.9% was used after a few freeze–pump–thaw cycles. The xenon sample, specified purity of 99.9995% was further purified by passing it through a hydrox. purifier (Matheson 8301) to eliminate water and air contaminants to better than a 0.1 ppm. This latter precaution was necessary since in many of the studies the Cl_2 concentration in the sample was of order 1ppm.

In the range of pressures studied, the pressure–density relationship for xenon is highly nonlinear, and a strong function of temperature. It is therefore important to relate the measured experimental pressures to density by an accurate equation of state. To this end we have used the equation of state given by Rabinovich *et al.*, which is based on a rather complete compilation of thermodynamic data on rare gases:[22]

$$\frac{p}{\rho RT} = 1 + \sum_{i=1}^{8} \sum_{j=0}^{5} b_{ij} \left(\frac{T}{T_{cr}}\right)^{-j} \rho^{i}$$

in which ρ = density, p = pressure, T = temperature, T_{cr} = critical temperature, and b_{ij} are the coefficients of the equation of state. For the sake of convenience in the interpretation of the data to be presented, a plot of density vs pressure is given in Fig. 1. The strong temperature dependence of the pressure requires precise control of cell temperature. The critical density, pressure, and temperature for xenon are: 1.110 g/cc, 57.6 atm, 289.7 K. At room temperature, the critical density is reached at a pressure of 67 atm. The cell design, limited by the window burst pressure, allowed safe operation at pressures as high as 200 atm. Our data were taken at densities as high as 2 g/cc, nearly twice the critical density, and two thirds of the density of the solid.

Several laser excitation sources were used in the course of these studies. The 308 nm output of a gas phase XeCl laser was used most commonly. While this yielded very high densities of the triatomic exciplex, its time profile of ~25 ns followed by an afterpulse, limited the measurements of the fastest relaxation data. This pulse profile is however useful for the diagnosis of the nonlinear photogeneration mechanisms, as will be discussed below. In most studies, emission spectra and lifetimes were measured simultaneously. The spectra were recorded with an optical multichannel analyzer equipped with a 1/4 m polychromator and 1024 element intensified diode array (EG&G OMA III). Lifetimes were measured by collecting fluorescence at right angle to the excitation beam through a 1/4 m monochromator, with a PMT (Hamamatsu R666), and recorded with a digitizing/

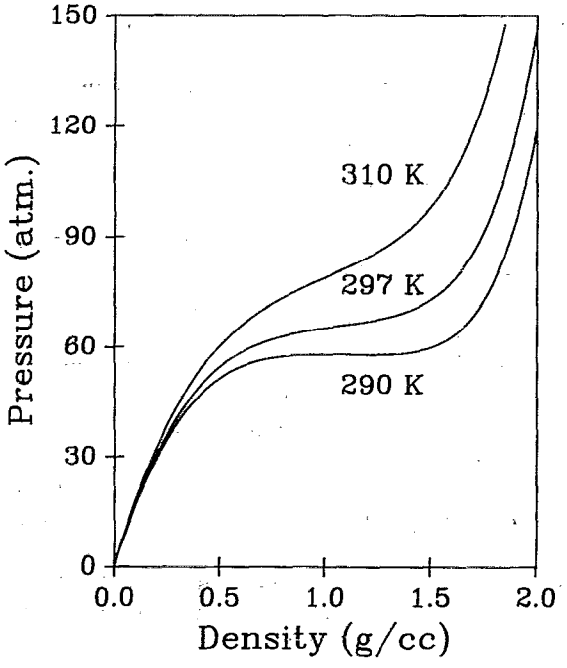

FIG. 1. Pressure vs density relation for Xe near room temperature. The curves, shown for three different temperatures, were calculated according to the equation of state given in Ref. 18.

averaging scope (Tektronix 2440). The response time of this train was ~3 ns, shorter than pulse widths of the excitation sources.

III. RESULTS

Two photon excitation of Cl_2/Xe mixtures—gaseous, liquid, or solid—near 300 nm, leads to the production of the xenon chloride exciplexes.[23] These excited state charge transfer complexes can be conveniently monitored by their luminescence. In low pressure xenon, emission from both the diatomic and triatomic xenon chloride can be observed, while at high xenon pressures, due to the efficient three-body reaction:

$$Xe^+ Cl^- + 2Xe \rightarrow Xe_2Cl + Xe \qquad (1)$$

emission from only the triatomic is seen. The three-body cross section of Eq. (1) has previously been measured[24] to be 1.2×10^{-30} cm^6 s^{-1}. Therefore at 1000 Torr, the reactive quenching rate of the diatomic exciplex is $\sim10^9$ s^{-1}, much faster than the effective radiative relaxation rate, 5×10^7 s^{-1}, of the diatomic B/C states.[17,24] This is illustrated in Fig. 2 in which emission spectra from Cl_2/Xe samples at different Xe pressures are shown. In the low pressure sample, at 686 Torr [trace (d) of Fig. 2], a portion of the diatomic $C\rightarrow A$ emission is seen (the blue cutoff of this spectrum is due to an acetone filter used to eliminate laser scatter). At higher pressures [traces (a), (b), and (c) of Fig. 2], the reactive interconversion of the diatomic is too fast to observe any emission from the B or C states.

As illustrated in Fig. 2, the triatomic exciplex emission spectra are broad. The breadth is due to the the bound-to-free nature of these transitions. The width of the emission band, and its maximum are plotted as a function of Xe density in Figs. 3(a) and 3(b), respectively. The bandwidth, 0.51 eV at zero pressure, undergoes a slight narrowing as a function of increasing Xe pressure (a change of 0.02 eV over a range of 150 atm). The emission peak undergoes a large red shift, ~0.27 eV, in the same range.

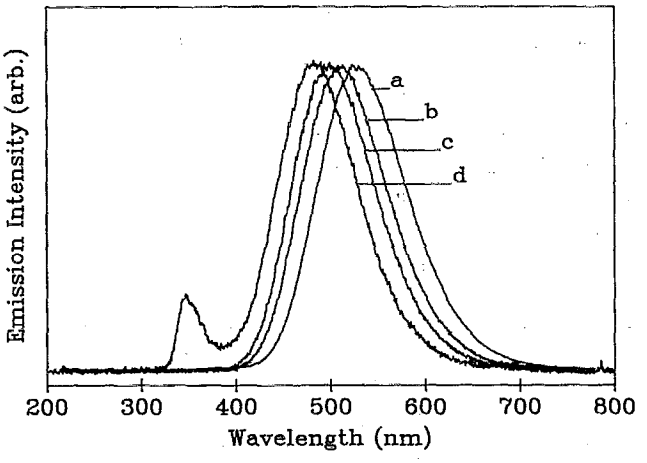

FIG. 2. Representative emission spectra of $Xe_2Cl(4\,^2\Gamma)$ in gaseous and supercritical fluidxenon. The spectra are from room temperature samples excited at 308 nm. The sample compositions are: (a) $Cl_2 = 1.02$ Torr, Xe = 1.811 g/cc (102 atm); (b) $Cl_2 = 0.22$ Torr, Xe = 0.398 g/cc (49 atm); (c) $Cl_2 = 0.11$ Torr, Xe = 0.195 g/cc (30 atm); (d) $Cl_2 = 0.99$ Torr, Xe = 0.0048 g/cc (0.90 atm).

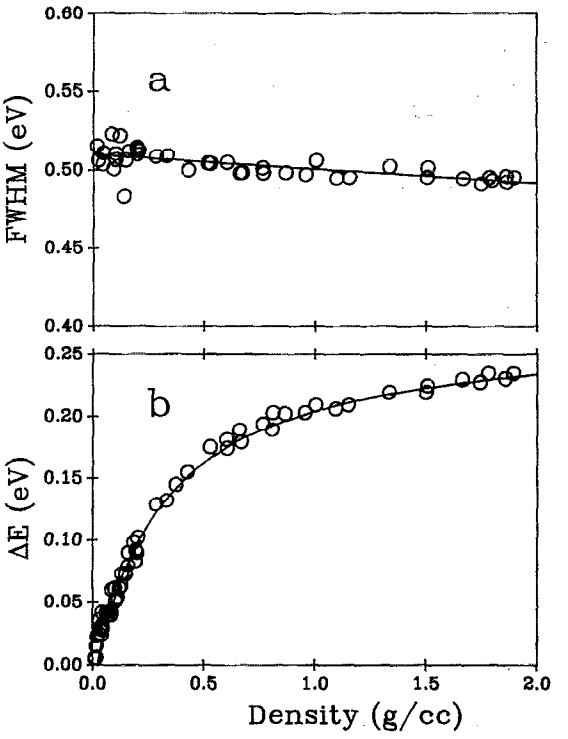

FIG. 3. (a) Dependence of the Xe_2Cl emission linewidth, FWHM, on Xe density. The data are from room temperature samples, excited at 308 nm, with different Cl_2 content (Cl_2 partial pressures ranging from 0.01 to 4.5 Torr). (b) Dependence of the Xe_2Cl emission line shift on Xe density. The shifts of the emission band maxima from their zero pressure value, 2.589 eV (479 nm), are plotted vs the density of added xenon. The data are from the same samples as in (a). The continuous curve is the best fit of the data to the form of Eq. (7a) in text.

Emission spectra were also recorded for several densities as a function of temperature. The lower limit in the range of temperatures was dictated by the boiling point of a given sample, the upper limit was maintained below ~335 K to avoid reactivity at the cell walls. These results, the temperature dependence of band maxima and widths, are summarized in Figs. 4(a) and 4(b), respectively. In this narrow range of temperatures, the line shift shows a nearly linear inverse dependence on temperature, with slopes that depend on density. A linear dependence of linewidths on temperature is observed in the same temperature range. The linear fit shown in Fig. 4(b) yields a slope of $-9.4(\pm0.4)\times10^{-4}$ eV/K, and an intercept of $0.25(\pm0.01)$ eV. The latter value is within experimental error, the same as that measured in 12 K matrices.[25]

Lifetime measurements were made for samples with different composition. The measurements were made in two different modes: (a) pressurization, or constant Cl_2 measurements—in which after introducing a fixed amount of Cl_2 in the cell, Xe is gradually added; (b) depressurization, or constant mole fraction measurements—in which the gas mixture at high density is initially prepared and subsequently let out of the cell. Given the large range of densities that were studied, the data are presented on two different abscis-

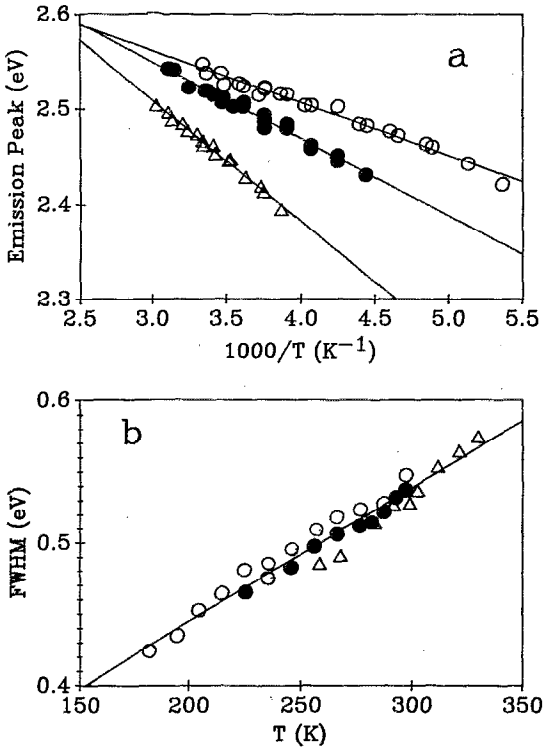

FIG. 4. (a) Temperature dependence of the Xe_2Cl emission band maximum. The band maxima, in eV, are plotted as a function of $1/T$. The data are from samples containing 1 Torr Cl_2, and different pressures of Xe. The xenon pressures (densities) and the coefficients of the linear fits, intercept and slope, for the three sets of data are: open circles: 3 atm (0.016 g/cc), 2.73–5.5$\times 10^{-5}$ eV K; filled circles: 11 atm (0.064 g/cc), 2.79–8.1$\times 10^{-5}$ eV K; open triangles: 28 atm (0.815 g/cc), 2.89–1.27$\times 10^{-4}$ eV K. (b) Temperature dependence of emission band width. The data were obtained from the same samples as in (a). The best fit line to all points, yields an intercept of 0.25 eV and a slope of 9.4$\times 10^{-4}$ eV/K.

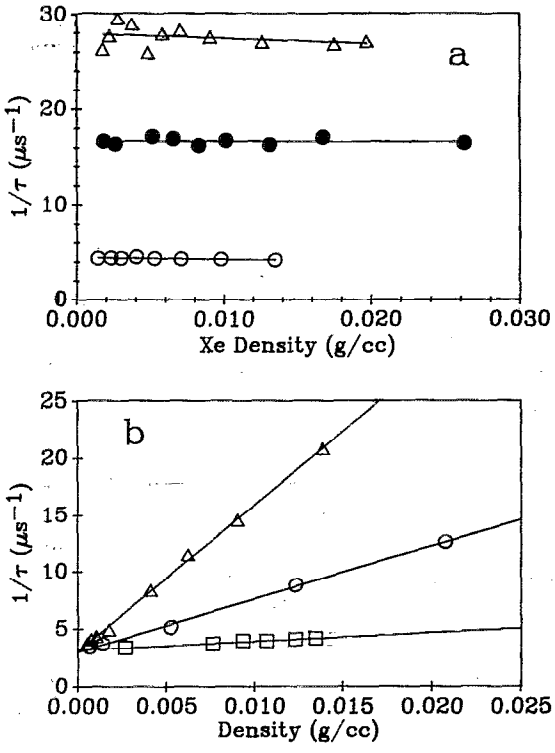

FIG. 5. Low pressure relaxation rates. (a) Fluorescence decay rates of Xe_2Cl as a function of Xe density. The Cl_2 partial pressures in the three sets of data are: open circles = 0.05 Torr, filled circles = 0.54 Torr, open triangles = 0.99 Torr. (b) Fluorescence decay rates of Xe_2Cl as a function of overall density. The data are obtained during depressurization of constant mole fraction samples. The Cl_2:Xe ratio in the three sets of data are: open squares = 1:38 000, open circles = 1:6900, open triangles = 1:2800.

sa. The low pressure measurements, pressures up to 5 atm, are presented in Fig. 5—pressurization in Fig. 5(a), and depressurization in Fig. 5(b). The effect of adding Xe in this low pressure range is barely perceptible; but the trend in all cases points at a negative slope, i.e., elongation of measured lifetimes with the addition of Xe. The depressurization data, taken at three different mole fractions show a linear dependence on overall density in this range, with a common intercept at 328($\pm$ 20) ns. The high density results are presented in Fig. 6. Note that the pressurization data in this range of densities, Fig. 6(a), clearly show an inverse dependence of the exciplex relaxation rate on Xe density.

IV. DISCUSSION

A. Photogeneration

While the exact description of the photoprocesses that lead to the generation of the exciplexes was not the aim of these studies, some insight in these mechanisms is helpful for the interpretation of the relaxation data. The majority of the relaxation measurements were conducted at 308 nm. At this wavelength, and at moderate Xe densities, there formally are two two-photon entrance channels in the formation of the XeCl exciplex. These are (a) photodissociation of molecular chlorine, followed by photoassociation of the atoms:[15,23]

$$Cl_2 + h\nu \rightarrow Cl + Cl, \quad (2)$$

$$Cl + Xe + h\nu \rightarrow Xe^+ Cl^-; \quad (3)$$

(b) two-photon induced harpooning:[17,26]

$$Cl_2 + Xe + 2h\nu \rightarrow Xe^+ (Cl_2)^- \rightarrow Xe^+ Cl^- + Cl; \quad (4)$$

the ejected neutral chlorine atom via this mechanism can also undergo photoassociation according to Eq. (3) above.

The 308 nm laser pulse width of $\sim$25 ns FWHM, is long compared to collisional time scales in these systems. Moreover, when the resonator is critically aligned, the main pulse is followed by an afterpulse which contains a significant intensity. Sequential photoabsorption processes—(2) followed by (3), or (4) followed by (3)—become very likely with these long pulses specially at high Xe densities. The time evolution of a 308 nm laser pulse, and the emission of the triatomic exciplex are shown in Fig. 7 at three different Xe pressures. Note that while the laser afterpulse is much smaller, the emission shows a double peak with the second peak dominating at higher pressures. The prominence of the second emission peak is taken as evidence for the presence of an efficient one-photon photoassociative generation of the exciplex from atomic Cl and Xe, following the photogeneration of Cl atoms in the main pulse. Either mechanism, Eq. (2) or (4), followed by the photoassociation process of Eq. (3), could explain this observation; and both mechanisms are thought to be operative. Power dependence measure-

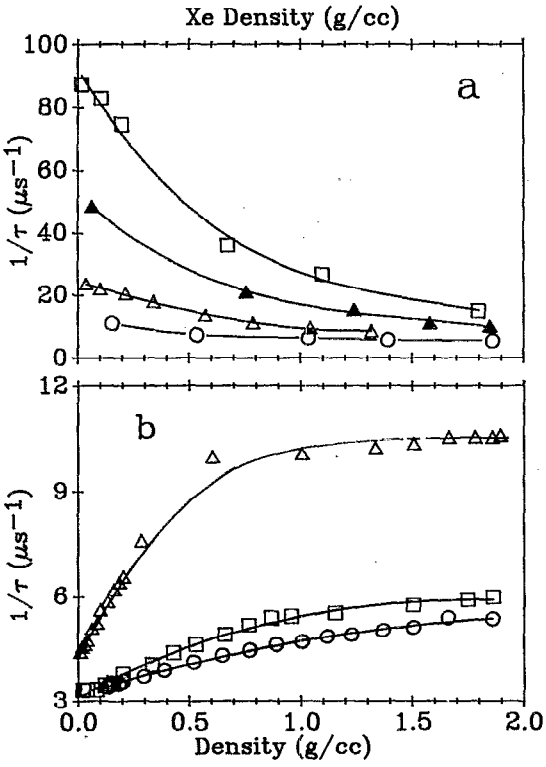

FIG. 6. High pressure relaxation rates, excitation at 308 nm with XeCl laser. (a) Fluorescence decay rates of Xe_2Cl as a function of Xe density. The Cl_2 partial pressures in the four sets of data are: open circles = 0.47 Torr, open triangles = 1.02 Torr, filled triangles = 1.98 Torr, open squares = 4.50 Torr. (b) Fluorescence decay rates of Xe_2Cl as a function of overall density. The data are obtained during depressurization of constant mole fraction samples. The Cl_2:Xe ratio in the three sets of data are: open circles = 1:470 000, open squares = 1:330 000, open triangles = 1:130 000.

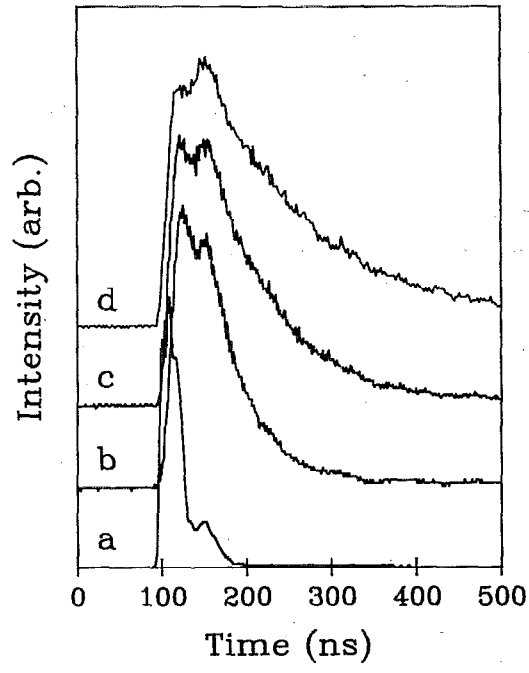

FIG. 7. Time profiles of (a) 308 nm laser pulse, and Xe_2Cl emission from a 1 Torr Cl_2 sample at Xe pressures of: (b) 8 atm (0.043 g/cc), (c) 57 atm (0.577 g/cc), (d) 70 atm (1.396 g/cc).

ments cannot distinguish between the two mechanisms. In both cases at low powers a second order dependence is to be expected, while at high powers a 3/2 order is to be expected (2 exciplexes per 3 input photons). The observed power dependence, which is illustrated in Fig. 8, fits this expectation. The observation of saturation, implies that Cl_2 is effectively depleted in the beam volume. In more recent two-laser experiments, the photoassociation channel has been directly demonstrated at Xe pressures ranging from 50 Torr to the critical pressure of Xe at 57 atm.[23] In these experiments a 345 nm laser is used as the initial photogeneration pulse, and a second doubled dye laser is delayed and used for the photoassociation step. Moreover, the time delayed two-color studies establish that both coherent and sequential two-photon generation of the exciplex is possible at high densities. The two-photon harpoon mechanism has previously been demonstrated by Setser and co-workers[17,26] for this same system in the gas phase, and in our laboratory for several other systems in condensed media.[2]

B. Clustering

Emission spectra of exciplexes have been studied in both liquid[18,27] and solid phases.[5,25] In the case of Xe_2Cl, the solid state measurements have been extended to pressures as high as 150 kbar.[21,28] The emission undergoes a large red shift which is primarily attributed to the ionic-to-covalent nature of exciplexic transitions, and solvation of the excited state dipole. No evidence has been found for a change in structure or nature of the ionic excited state. The observed

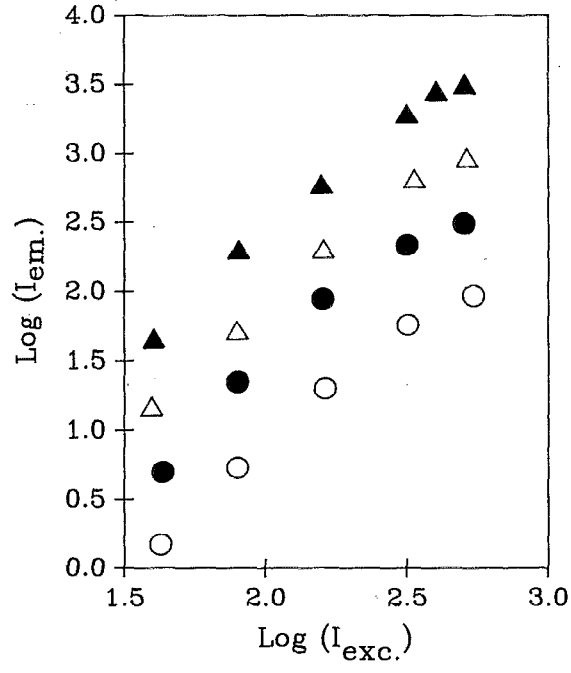

FIG. 8. Power dependence of Xe_2Cl emission. The data are obtained by 308 nm excitation of a sample containing Cl_2 at 1 Torr partial pressure and different Xe densities: open circle = 0.037 g/cc, filled circle = 0.35 g/cc, open triangle = 0.787 g/cc, filled triangle = 1.04 g/cc. The ordinate is in arbitrary units. The highest fluence points along the abscissa correspond to 2 MW/cm^2.

spectral shift of ~ 0.27 eV in the present studies [see Fig. 3(b)] should be interpreted by specific interactions. Given the large dipole of the exciplex (12.21 D), and the significant polarizability of xenon (3.99 Å^3), clustering of the exciplex with the buffer gas by three-body collisions is to be expected, viz:

$$Xe_2Cl + 2Xe = Xe_2Cl \cdot Xe + Xe. \tag{5}$$

The dimerization of xenon has been studied experimentally, and an equilibrium constant of 2.27×10^{-22} cm^3 has been deduced, i.e., at 1 atm, $\sim 0.6\%$ of Xe is in the form of Xe_2.[29] Thus, since Xe readily forms dimers even at moderate densities, the three-body collision probabilities are sufficiently large to establish the equilibrium implied in Eq. (5) during the lifetime of the exciplex, in the range of pressures of the data reported here. Given the short range nature of dipole–induced dipole interactions, the main contribution to the spectral shift would arise from such clusters, as opposed to changes in the bulk dielectric of the medium. Indeed, the density dependence of spectral shifts shown in Fig. 3(b) can be related to the extent of clustering. Defining an equilibrium constant for the formation of the one-to-one adduct, as in Eq. (5):

$$K_1 = \frac{[Xe_2Cl \cdot Xe]}{[Xe_2Cl][Xe]} \tag{6}$$

in which square brackets are used to indicate number densities, the observed spectral shift may be expressed as

$$\Delta E = \Delta E_\infty \frac{K_1[Xe]}{1 + K_1[Xe]} \tag{7a}$$

$$= \Delta E_\infty \frac{\delta \ln(Z)}{\delta \ln([Xe])}. \tag{7b}$$

In which ΔE_∞ corresponds to the spectral shift at saturation, i.e., the limit of complete clustering; and Z is the partition function of Xe_2Cl in all of its forms (Xe_2Cl and $Xe_2Cl \cdot Xe$ in the present case). The fit of the data to the form of Eq. (7a) is shown in Fig. 3(b). The best-fit parameters are: $\Delta E_\infty = 0.271$ eV ($E_0 = 479$ nm and $E_\infty = 535$ nm for the asymptotic limits of the emission maxima at low and high densities, respectively), and $K_1 = 6.8 \times 10^{-22}$ cm^3.

The equilibrium constant and energy shift determined above cannot be uniquely attributed to a one-to-one adduct. Since clustering is assumed to be due to dipole–induced dipole interactions, we may suspect that clusters with multiple adatoms can occur. In fact, since the dipole is along the Xe_2^+–Cl^- coordinate, the lowest energy binding site for a Xe atom is on the face of the triangle, of which there are two. It is then possible to extend the above treatment with the definition

$$K_n = \frac{[Xe_2Cl \cdot nXe]}{[Xe_2Cl \cdot (n-1)Xe][Xe]}. \tag{8}$$

Under the assumption of equivalent binding sites, $K_1 = K_2 = K_n = K$, and accordingly equal incremental shifts per added Xe atom, the spectral shift expression reduces to the same form as in Eq. (7a):

$$\Delta E = n\Delta E_\infty \frac{K[Xe]}{1 + K[Xe]} \tag{9}$$

with the difference, that the asymptotic limit reached in this case is the sum of incremental energy shifts experienced per bound atom. In principle, the assumption of equivalence of sites can be relaxed. However, such a treatment would introduce additional parameters in the expression for ΔE, namely: different equilibrium constants and energy shifts for atoms bound in different solvation shells. Such information cannot be extracted from the experimental data which are already well fit by two parameters. However, contributions to the observed spectral shift for clusters with $n > 2$ are to be expected to be small. The equilibrium constant for binding in the second solvation shell will reduce dramatically since it depends exponentially on the binding energy, and the latter is strictly due to short range interactions: $K \propto \exp[-U(R^{-6})]$. Moreover, the spectral shift associated with such clusters is due to the differential stabilization of the excited state relative to the ground state, $\Delta E(R) = U'(R^{-6}) - U''(R^{-6}) = \Delta U(R^{-6})$. Therefore, at large R, the contribution to the average spectral shift can be expected to have an approximate R^{-12} dependence. It is therefore not too surprising that the two parameter fit to the data, either according to Eq. (7a) or (9) (with $n = 2$), is a good representation of the observed shift. According to the two equivalent-sites model, the spectral shift per bound Xe is 0.135 eV. This should be regarded as an upper limit, since contributions to the shift from clusters with $n > 2$ are ignored in the treatment.

The reduction in spectral width as a function of Xe density shown in Fig. 3(a) can be rationalized within the framework of clustering. The exciplexic emission is from a bound to a strictly repulsive potential. Therefore, any increase in equilibrium bond length, along either Xe–Xe or Xe_2–Cl coordinates, will lead to radiation to a less steep part of the ground state potential surface, and therefore to a narrower spectral distribution in emission. The same consideration would lead to the expectation of spectral narrowing with the lowering of vibration temperatures. The density and temperature dependence of the spectral width is consistent with these expectations. Extension of the ionic bond is to be expected upon clustering, since the long-range part of electrostatic potentials is softened by solvation, while the repulsive wall remains unaffected. The exact magnitude of this effect is difficult to extract from the data, since a significant portion of the emission is due to vibrationally excited states. As shown in Fig. 4(b), the spectral width reduces as the temperature is lowered, as would be expected from bound-to-repulsive transitions. We point that in 12 K solid Xe, it has been possible to simulate the emission spectrum of Xe_2Cl by a two-dimensional classical reflection approximation, using pairwise additive gas phase potentials.[25] While such spectral inversions are not unique, it can be stated that the spectral narrowing data with density and temperature are consistent with the simple electrostatic clustering model presented above.

The temperature dependence of the spectral shift could in principle provide an additional test for the clustering model proposed above. However, the utility of this data is very limited since the measurements are conducted under isochoric conditions. According to Eq. (9), the free energy

of the clustering equilibrium can be extracted from the spectral shifts:

$$\frac{\Delta G}{kT} = \ln([\mathrm{Xe}]) + \ln\left(\frac{n\Delta E_\infty - \Delta E}{\Delta E}\right) \tag{10}$$

since $\Delta G = \Delta G(T,P)$, temperature and pressure effects cannot be separated in isochoric measurements. Nevertheless, if the data of Fig. 4(a) are recast in the form of Eq. (10), by plotting the right-hand side of Eq. (10) vs $1/T$, approximate ΔG values can be extracted from linear fits. For Xe pressures of 3, 11, and 28 atm at room temperature, ΔG values of 0.08, 0.117, and 0.17 eV are obtained. The strong dependence of the free energy on pressure, is a good indication to the effect that the equilibrium entails a large change in molecular volumes, as would be expected in clustering equilibria. We also note that the free energy values bracket the ΔE_∞ value of 0.135 eV extracted from the fit of the density dependent shift.

Given the qualitative agreement of all the spectroscopic data with the clustering model, we next calculate the equilibrium constant predicted by the electrostatic binding model advanced above. The equilibrium constant in Eq. (6) can be computed according to statistical theory, as

$$K_{AB} = \frac{sQ^{AB}}{Q^A Q^B} e^{E/kT} \tag{11}$$

in which Q denotes the partition function for a given species; A and B refer to the exciplex and Xe, respectively; E represents the binding energy of the complex; and $s = 2$ is the symmetry number. An equilibrium structure, binding energy, and vibrational partition function for the cluster are necessary to evaluate K_{AB}. A simple binding model is assumed for these estimates. For the exciplex, a rigid triangular geometry, with the Xe atoms at the base and the Cl atom at the apex, is assumed. For the base of the triangle (Xe–Xe distance) 3.17 Å is assumed, while for the height (Xe_2–Cl) distance, 3.00 Å is assumed. These values are derived as the best set of parameters from different theoretical estimates and have previously been employed to simulate solid state emission spectra with good success.[25] Partial charges, $q = 0.85\ e^-$, are placed on the Cl atom and midpoint between the Xe atoms, to reproduce the theoretically determined dipole of the exciplex[4] of 12.21 D. The potential between the exciplex and Xe is constructed as a sum of terms:

$$V(\mathrm{Xe_2Cl\text{–}Xe}) = V(\mathrm{Cl^-\text{–}Xe}) + 2V(\mathrm{Xe\text{–}Xe}) + V(q^-\text{–}\mathrm{Xe}) + V(q^+\text{–}\mathrm{Xe}) \tag{12}$$

in which $V(\mathrm{Cl^-\text{–}Xe})$ retains the exponential repulsion and R^{-6} attraction term of a previously reported Cl^-–Xe potential[30] which we fit to the form: $A\exp(-aR) - A6/R^6 - A4/R^4$ ($A = 64\,367.8$ eV, $a = 4.07$ Å^{-1}, $A6 = 57.3$ eV Å^6, $A4 = 29.12$ eV Å^4); for V(Xe–Xe) a 6-12 potential is assumed[31] with $\varepsilon = 0.0199$ eV and $\sigma = 3.98$ Å, the last two terms in Eq. (12) are charge induced dipole terms which are explicitly evaluated for the $0.85\,e^-$ partial charges: $V = \alpha q^2/2(\mathbf{r}_+/r_+^3 - \mathbf{r}_-/r_-^3)^2$ in which α is the polarizability of Xe, and $\mathbf{r}_+$ and $\mathbf{r}_-$ are the vector positions of the fixed partial charges from the clustering Xe atom ($\alpha q^2/2 = 21.04$ eV Å^4). A grid search is then performed to find the potential minimum. The minimum yields a binding energy of 0.098 eV, which occurs at a Xe distance of 3.498 Å above the exciplex plane and at a height of 1.755 Å from the base of the triangle. The vibrational frequencies for the clustered atom were then calculated as 35, 20, and 13.5 cm^{-1} for motions perpendicular to the exciplex plane, parallel, and perpendicular to the exciplexic dipole, respectively. Using the rigid geometry for the complex, the moments of inertia were calculated ($I_a = 2.15\times10^{-37}$, $I_b = 1.87\times10^{-37}$, $I_c = 3.73\times10^{-38}$ in units of g cm^2). Using these classical partition functions, the equilibrium constant for the one-to-one adduct, Eq. (11), can be computed as $K_{AB} = 1.28\times10^{-22}$ cm^3, at room temperature.

Given the approximations made in the above determination, the factor of 5 difference between the calculated equilibrium constant, and that determined from the spectral shifts seems acceptable. At the minimum geometry of the cluster in the excited state, the contribution of the Xe atom to the ground state potential is negligible. As such, the calculated binding energy of 0.098 eV should closely correspond to the spectral shift of the clustered species, which was determined as 0.135 eV in the two equivalent-sites interpretation of the experimental data. Given the fact that only electrostatic binding due to point charges is assumed in the calculation, the calculated binding energy is expected to be an underestimate. If instead, the experimental energy shift is used for E in Eq. (11), then an almost exact agreement between experiment and calculation would be obtained for the equilibrium constant. We thus conclude that the spectral data as a function of density and temperature are consistent with clustering of the exciplex with Xe atoms, such that at saturation at least two Xe atoms are added to equivalent sites—one on each face of the exciplex plane. The computed equilibrium constant and that extracted from spectral shifts, are expected to be lower and upper bounds to the true value. As such, it is possible to conclude that at 1 atm of Xe, between 0.3% and 2% of the exciplexes are clustered with one Xe.

C. Radiative lifetime

The radiative lifetime of Xe_2Cl has been measured by several different groups previously. The first report is due to Tang and co-workers,[6] who found a value of 100 ns. Subsequent studies revised this value upward to 185 ns,[13] to 210 ns,[14] to 245 ns,[15] and recently, to 300($\pm$50) ns.[16] The theoretical value was calculated to be 330 ns.[4] The radiative lifetime of the exciplex in our studies is determined from several different measurements, the most direct being the low pressure measurements illustrated in Fig. 5. It can be seen in Fig. 5(a) that Xe, in the range of a few atmospheres, does not have a significant effect on observed fluorescence decay rates. In the same pressure range, the constant mole fraction data show a linear dependence on overall density, and yield a well defined intercept as illustrated in Fig. 5(b). The fluorescence decay rates in this range of densities are determined by the Cl_2 partial pressure, and therefore the intercept of 328($\pm$20) ns should represent the radiative lifetime of the exciplex. This determination is consistent with the theoretical value,[4] and within experimental error,

in agreement with those of Berman.[16]

Given that the lifetime determined in our experiments is longer than all previous measurements; and the fact that at the very low pressures decay rates longer than any of the previously reported radiative lifetimes is directly observed; we are tempted to trust 328 ns as a more accurate value for the radiative lifetime of the gas phase triatomic Xe_2Cl exciplex. Among the experimental considerations that may be responsible for the observation of the longer lifetime, purity of the gases and passivation of cell walls are thought to be the most important. The Xe gas used in our experiments was purified to a level of 0.1 ppm prior to use, and in our depressurization studies lifetimes are measured for samples containing Cl_2 pressures as low as ~ 0.01 Torr, hence little extrapolation is made to obtain the intercept values. Passivation of cell walls was carefully monitored in these studies, by verifying that signal intensities did not change over time—an acceptable level of passivation was only achieved after exposure of the cell walls to Cl_2 for periods longer than 12 h.

The above analysis is valid at low densities of Xe, where clustering considerations are unimportant. In the case of clustering, an elongation of the radiative lifetime due to reduction of the transition dipole is to be expected. A detailed treatment of this phenomenon has recently been presented.[32] The radiative decay rate of the clustered exciplex can be related to the free form as

$$\frac{1}{\tau} = \left(\frac{E}{E_0}\right)^3 \frac{|\mu|^2}{|\mu_0|^2} \frac{1}{\tau_0} \tag{13}$$

in which E represents the emission energy, μ represents the transition dipole, and the subscript 0 is used for the free exciplex. In the present case, to a good approximation, the transition dipole can be identified with the excited state dipole. Within the spirit of the clustering equilibrium calculation of the previous section, if we assume a point polarizable Xe atom, and a point dipole on the exciplex, the total dipole of the complex can be estimated as the difference between the molecular dipole and the dipole–induced dipole: $\mu = \mu_0(1 - \alpha/r^3)$, where r is the distance between Xe and the dipole, and α is the polarizability of Xe. Using the experimental spectral shift, and r calculated in the previous section, it is possible to estimate that the radiative relaxation rate of $Xe_2Cl \cdot Xe$ and $Xe_2Cl \cdot 2Xe$ would be reduced to 70% and 49% of that of the free exciplex, respectively. This effect is counteracted by the increase in the bulk dielectric of the medium at high densities. A commonly accepted relation between radiative rates in vacuum and a dielectric continuum is[33]

$$\frac{1}{\tau} = \frac{n(n^2+2)^2}{9} \frac{1}{\tau_V} \tag{14}$$

in which n is the index of refraction of the medium, and the subscript v is used for vacuum. Using the Lorentz–Lorenz relation, n can be well estimated. At the highest densities of the present studies, at 2 g cm^{-3}, $n = 1.23$. Accordingly, an increase in radiative decay rates of $\sim 68\%$ is expected. Although these estimates are approximate, it should be clear that at high densities, the effects of clustering and bulk dielectric on radiative lifetimes nearly cancel each other. In the low pressure data of Fig. 5, no evidence for changes in radiative lifetimes is discerned. The effect should be most pronounced in samples of low Cl_2 content, in which the fluorescence decay is dominated by radiation. To the contrary, the slight negative slope for decay rates as a function of added Xe is in the sample with the highest Cl_2 concentration [open triangles in Fig. 5(a)], which would imply that the effect of added Xe is the reduction in efficiency of quenching by Cl_2. In what follows, we assume that the radiative lifetime of the exciplex remains unchanged in the studied range of densities.

D. Relaxation kinetics at low pressures

The relaxation kinetics of both diatomic and triatomic xenon chlorides have been previously studied. In the case of the triatomic the pertinent relaxation rates that had been previously reported are

(i) deactivation by Cl_2:

$$Xe_2Cl + Cl_2 \rightarrow 2Xe + Cl + Cl_2, \tag{15}$$

with a rate constant $k^d(Cl_2)$ which has been determined to be essentially gas kinetic by all previous measurements—the reported values[6,15] range from 2.2×10^{-10} to 4×10^{-10} $cm^3\,s^{-1}$:

(ii) deactivation by Xe:

$$Xe_2Cl + Xe \rightarrow 3Xe + Cl. \tag{16}$$

All previous determinations of the rate of this process have been limited to low pressure studies (few atmospheres), a range in which the effect of xenon is not measurable [see Fig. 5(a)]. While there exist prior reports of this rate constant,[13] most researchers establish only an upper bound. According to our low pressure data, the effect of addition of xenon may result in a slight elongation of the exciplex lifetime. This is somewhat obvious in the samples with the highest Cl_2:Xe mole fractions [see Fig. 5(a)]. Moreover, at the highest pressures of Xe used in the present work, and for samples containing $\leqslant 0.5$ Torr of Cl_2, the exciplex relaxation is essentially radiative. Thus, in what follows, we will assume that $k^d(Xe) = 0$.

If we ignore the contributions to deactivation by Xe, then the measured lifetimes in Cl_2/Xe mixtures at low pressures should be given by

$$1/\tau = 1/\tau_r + [Cl_2]k^d \tag{17}$$

in which $k^d = k^d(Cl_2)$, and $[Cl_2]$ is the original number density of Cl_2. Thus from the slopes of the linear fits to the data in Fig. 5(b), a deactivation rate constant of $7(\pm 1)\times10^{-10}$ $cm^3\,s^{-1}$ is obtained. The major source of error in this determination is the uncertainty in the Cl_2 number density due to wall effects. This rate constant is larger than all prior determinations, the largest previously reported value being $5.2(\pm 0.2)\times10^{-10}$ $cm^3\,s^{-1}$ (see Table I of Ref. 16). To be exact, the density dependence of the radiative lifetime should be included in Eq. (17). However, as can be seen in Fig. 5(b), the dependence of deactivation on density is quite linear, as such only k^d can be extracted.

E. Relaxation kinetics at high densities

The most striking observation in the lifetime studies are those represented in Fig. 6. Namely, an inverse dependence of deactivation rates on Xe density is observed at high densities. The origin of this inverse dependence can be uniquely identified: since Xe does not deactivate the exciplex, at high pressures it acts as a buffer that reduces the encounter probability between the exciplex and its quencher, namely molecular Cl_2. This interpretation is quantified below.

It was established from the low pressure studies that deactivation of the exciplex by molecular Cl_2 proceeds with greater than gas kinetic probability, and that Xe does not deactivate the exciplex. At low pressures, the encounter probabilities are given by gas kinetic collision rates, $Z_k = \sigma\langle v\rangle n$ (σ = collision cross section, $\langle v\rangle$ = average velocity, n = number density of collision partner). This treatment is valid as long as the mean free path between collision partners is much larger than the interparticle separations. At a density of 1 g cm^{-3}, midrange of the studies, the average distance between atoms in the fluid is only 6 Å. At such densities, encounter probabilities are diffusion controlled, $Z_D = 4\pi RDn$ (R = diameter of diffuser, D = diffusion coefficient). In order to account for the entire density range of the present studies an expression for encounter probabilities that span the gas kinetic and diffusive limits is necessary. If we note that these two different processes constitute parallel channels, then the total encounter probability Z can be related to the two channels through

$$1/Z = 1/Z_k + 1/Z_D. \tag{18}$$

To a first approximation, and at moderate densities, the diffusion coefficient is inversely proportional to the density of the medium, which in the present studies is given by the density of xenon. With this assumption, the deactivation rate of the exciplex can be expressed as

$$1/\tau = 1/\tau_r + Z_k Z_D p[\mathrm{Cl_2}]/(Z_k + Z_D), \tag{19a}$$

where

$$Z_D = 4\pi RD_{12} = C/[\mathrm{Xe}] \tag{19b}$$

in which D_{12} is the diffusion coefficient of Cl_2 in Xe. A convenient expression for the analysis of data, in particular for the case of pressurization studies, can be obtained by recasting the above expression as

$$[\mathrm{Cl_2}]/(1/\tau - 1/\tau_r) = 1/k^d + [\mathrm{Xe}]/C \tag{20}$$

such a plot, normalized lifetime vs Xe density, is shown in Fig. 9(a) for the data of Fig. 6. The data are well represented by Eq. (20)—the model clearly contains the essence of the controlling kinetics. From the intercepts of the linear fits to Eq. (20), k^d can be obtained, while C can be obtained from the slopes. This method of analysis of the entire pool of data (not all shown here), yields an average value of $C = 7.9(\pm 0.5)\times 10^{-13}$ s and a value for deactivation by Cl_2 of $k^d = 7(\pm 1)\times 10^{-10}$ cc s^{-1}.

The diffusive encounter coefficient C as defined in Eq. (14) can be estimated from gas kinetic treatments for mutual diffusion:[31]

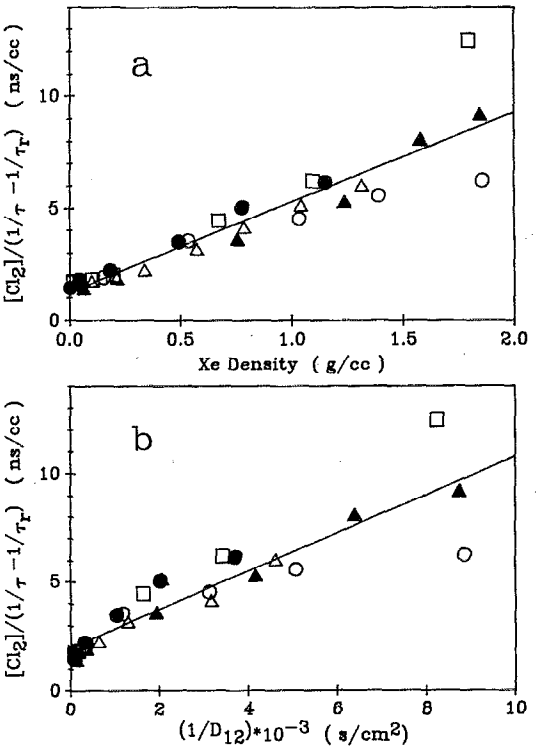

FIG. 9. Normalized decay times of Xe_2Cl as a function of (a) Xe density, (b) inverse diffusion coefficient. The Cl_2 partial pressures in the five data sets are: open circle = 0.47 Torr, filled circle = 0.89 Torr, open triangle = 1.02 Torr, filled triangle = 1.98 Torr, open square = 4.50 Torr. Excitation at 308 nm.

$$D_{12} = 6.43\times 10^{16}\frac{(T^3/2m)^{1/2}}{[\mathrm{Xe}]\sigma^2\Omega_{12}(T^*_{12})^{(1,1)^*}} \tag{21}$$

in which m is the reduced mass of Cl_2–Xe pair, $\sigma = (\sigma_1 + \sigma_2)/2 = 4.228$ Å is the sum of Lennard-Jones radii obtained from diffusion measurements,[31] and Ω_{12} is the scattering integral for first-order correction of cross sections.[31] Using $R = 4.2$ Å for the radius of the diffuser in Eq. (14b), $C = 1.27\times 10^{-12}$ s can be calculated. The agreement between this estimated value and that obtained from the experiment (0.8×10^{-12} s) should be regarded as good, in view of the simplified treatment used for mutual diffusion.

More elaborate, nevertheless empirical, treatments of diffusion have previously been used by Troe and co-workers for the analysis of kinetic data in similar systems (recombination in gaseous and supercritical fluids).[34] We have employed the several suggested methods for calculating D_{12} and analyzed the data according to Eq. (14) above (for more details see Ref. 35). While little new insight or improvement in fits are obtained by these different methods, we present the simpler of treatments here for the sake of completeness.

An exponential switching function has been suggested in Ref. 34:

$$\frac{kT}{\eta D_{12}} = 3\pi\sigma_1\left\{1 - \exp\left(-\frac{[\mathrm{Xe}]}{[\mathrm{Xe}]_{cr}}\right)\right\} \tag{22}$$

in which D_{12} is the low pressure diffusion coefficient as defined in Eq. (21), η is the low density viscosity, σ_1 is the

Lennard-Jones diameter of the diffuser, and $[\ ]_{cr}$ is the critical density of the solvent. The function allows for asymptotically reaching the Stokes–Einstein limit for diffusion at densities much higher than the critical. The improvements in such a treatment are to be derived at very high densities. The application of Eq. (22) requires the knowledge of density dependent viscosities, which are available for rare gases.[22] Using the known values of viscosity, D_{12} was calculated and the data analyzed according to Eq. (19). A plot of normalized lifetime vs $1/D_{12}$ are presented in Fig. 9(b). From the slope of the linear fit to the data a value for $1/4\pi R = 7.5(\pm 1.1)\times 10^5\ \mathrm{cm}^{-1}$ is obtained, i.e., a diameter for Cl_2 of 11 Å, a factor of 2.5 larger than expected. This discrepancy can be rationalized by noting that instead of mutual diffusion, this treatment is based on self-diffusion. From the intercept of the linear fit, a value of $k^d = 4.3(\pm 0.5)\times 10^{-10}\ \mathrm{cm}^3\ \mathrm{s}^{-1}$ is obtained, nearly a factor of 2 smaller than the values obtained by the simple diffusion treatment and those obtained directly from the low pressure data. Even though the smaller quenching rate by Cl_2 is more consistent with previous determinations, in the present analysis its validity is based on approximate empirical treatments of diffusion. A larger than gas kinetic quenching cross section is to be expected for this system based on the large dipole induced dipole potential that governs encounter cross sections between exciplex and Cl_2.

F. Transient loss measurements

The system kinetics, as described, has the qualifications of a high pressure exciplex laser. Population inversion is guaranteed due to the bound–free nature of the transition. The stimulated emission cross section of the triatomic transition can be estimated from its radiative lifetime and homogeneous emission bandwidth as $\sim 5\times 10^{-18}\ \mathrm{cm}^2$. Based on the observation of saturation in the power dependence measurements of the emission intensity, it is clear that the requisite number densities of order $10^{17}\ \mathrm{cm}^{-3}$ could be generated when the 308 nm pump beam was tightly line focused ($\sim 100\ \mathrm{MW/cm}^2$) in the high pressure cell. Yet no spectral collapse, which would be expected under conditions of amplified spontaneous emission, could be observed. Attempts at small signal gain measurements instead showed a strong attenuation of the probe beam. A typical example is illustrated in Fig. 10, together with the experimental geometry.

A T-cell was used for these measurements. The pump beam was line focused with a cylinder lens through a 1 in. sapphire window. The probe beam, taken from a separate excimer-pumped dye laser operating at 540 nm, was overlapped with the pump beam waist (see illustration in Fig. 10). The transmitted probe beam was spatially filtered by a pair of irises and monitored with a photodiode. The transmission intensity as a function of delay between the two lasers is shown in the lower panel of the figure. The emission intensity detected by the same diode after opening of the irises is also shown. As was discussed above, the emission is double peaked due to the afterpulse of the pump laser. These conditions were chosen since they are particularly well suited for the diagnosis of the loss mechanism. A comparison of the emission and transmission time profiles reveals that: (a) the loss sets in with the decay of the excited state and not with its rise, i.e., the loss mechanism is not optical in nature, as would be expected for transient absorptions from the excited state, (b) the loss has an onset time constant that is comparable to the relaxation time scale of the excited state, and as such the total loss is proportional to the integral of relaxed excited state population, (c) finally, the probe beam returns to its 100% transmission value on a time scale of several milliseconds. These observations would indicate that the loss mechanism is due to thermal shock of the system and the launching of acoustic waves. The ensuing turbulence is evidently sufficient to scatter the probe beam outside the observation zone. This mechanism, which is the result of the combination of kinetic energy release upon the radiative dissociation of the triatomic exciplex to the repulsive ground state, and the poor thermal conductivity of rare gas atoms, is thought to be the main loss mechanism in the system. Transient absorptions which have been seen in solid state Xe_2Cl are not clearly evident in the present.[36]

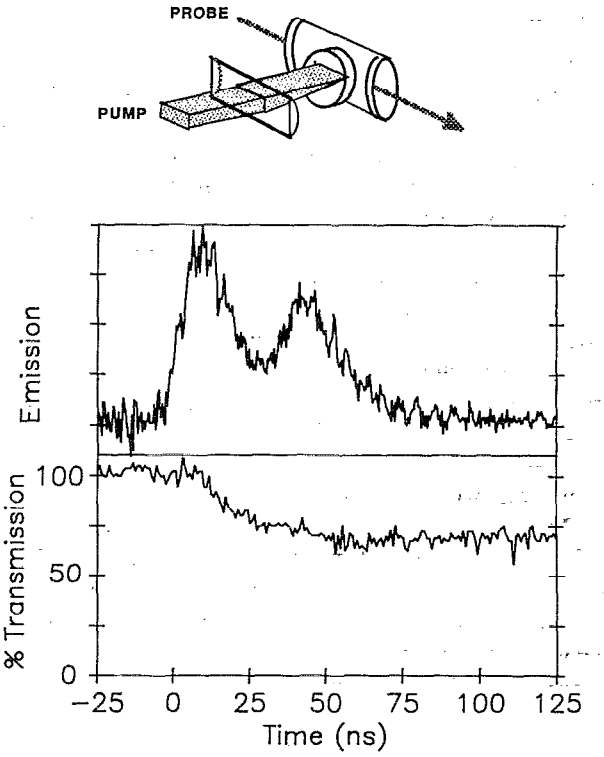

FIG. 10. Transient loss measurements. The pump (308 nm, 70 mJ) and probe (540 nm, 100 nJ) geometry of the measurements is shown at the top. The time profiles of the exciplex emission (upper panel) and the probe transmission (lower panel) are illustrated for a pump with a strong afterpulse (for the laser pulse shape see Fig. 7). Zero time corresponds to the edge of the pump pulse. The sample composition for this example was: $Cl_2 = 6$ Torr, and Xe = 25 atm.

V. CONCLUSIONS

Emission spectra of Xe_2Cl as a function of temperature and pressure provide compelling evidence to the effect that in the gas/fluid phase, the exciplex readily clusters with Xe.

The main contribution to the observed spectral shift is assumed to be due to the first solvation shell, composed of two Xe atoms—one on each side of the plain defined by the triatomic exciplex. The equilibrium constant, and stabilization energy obtained from the experimental data, 6.8×10^{-22} cm^3 and 0.135 eV, are in acceptable agreement with calculations of the same quantities, 1.28×10^{-22} cm^3 and 0.098 eV using classical partition functions and a geometry for the complex based on electrostatic binding of a point dipole to a point polarizable atom. The two determinations are expected to be upper and lower bounds of the true values. Complexation does not promote relaxation nor does it effect radiative lifetimes to any appreciable extent. In the pressure range of the studies, up to 150 atm, Xe acts as a buffer between the exciplex and Cl_2. Complexation in the gas phase, would imply that the same also occurs in liquids. As such, the present studies serve as direct proof of the postulates made to explain dynamical and spectroscopic observations in previous studies.[19,20]

The relaxation dynamics of Xe_2Cl in Xe can be treated with a simple model. Namely, efficient deactivation by Cl_2 with nearly twice gas kinetic cross section, and no deactivation by Xe. At high Xe densities the exciplex–Cl_2 encounter probabilities become diffusion controlled and therefore in dilute samples the relaxation is dominated by radiation. A rather simple model for this kinetics, which adequately reproduces the experimental observations, was presented. The model relies on the definition of a reduced encounter frequency, as a parallel process for diffusion controlled and gas kinetic encounter probabilities. Furthermore, the assumption is made that throughout the studied range, 50 Torr to 150 atm, the diffusion controlled encounter probability is inversely proportional to the density of Xe. A value for quenching by Cl_2, $k^d = 7.1(\pm1)\times10^{-10}$, and diffusion controlled encounter probabilities, $Z_D = 4\pi RD_{12} = 7.9\times10^{-13}/[\mathrm{Xe}]$, reproduce all of the data. The latter value was justified based on gas kinetic treatments of mutual diffusion. Little justification is found for resorting to more elaborate models in the studied range of densities.

The kinetic analysis has provided an upward revision for the radiative lifetime of the exciplex to 328($\pm$20) ns. This value, is in good agreement with the theoretical value,[4] and also within experimental error in agreement with a recent report of the same lifetime.[16]

Finally, it is clear from power dependence measurements that the triatomic exciplex can be efficiently generated in supercritical fluids. At pump fluences of the order of 100 MW/cm^2, Cl_2 exciplex number densities in excess of the required 10^{17} cm^{-3} are generated. Yet instead of positive gain, a transient loss due to optical scattering by shock waves generated by the radiative dissociation of the exciplex is observed. Such losses could in principle be overcome by faster pump sources, or corrected by phase conjugate mirrors. These issues have to be addressed in order to design viable lasers from the family of triatomic rare gas halides, since a common characteristic to all members is the excess kinetic energy, $\sim$1 eV, released upon the bound-to-free radiative transition.

ACKNOWLEDGMENTS

This research was supported by the United States Air Force Astronautics Laboratory under Contract No. F04611-87-K-0024, and by the National Science Foundation, Grant No. ECS-8914321. The scholarship given to F. O., by Nippon Mining Co., LTD. of Japan is gratefully acknowledged.

[1] D. L. Huestis, G. Marowsky, and F. K. Tittel, in *Excimer Lasers*, edited by Ch. K. Rhodes, in Topics in Applied Physics, Vol. 30 (Springer, New York, 1984), Chap. 6.
[2] M. E. Fajardo, R. Withnall, J. Feld, F. Okada, W. Lawrence, L. Wiedeman, and V. A. Apkarian, Laser Chem. **9**, 1 (1988).
[3] R. Sauerbrey, Y. Zhu, F. K. Tittel, and W. L. Wilson, Jr., J. Chem Phys. **85**, 1299 (1986).
[4] W. J. Stevens and M. Krauss, Appl. Phys. Lett. **41**, 308 (1981).
[5] M. E. Fajardo and V. A. Apkarian, J. Chem. Phys. **89**, 4102 (1988).
[6] K. Y. Tang, D. C. Lorents, and D. L. Huestis, Appl. Phys. Lett. **36**, 347 (1980).
[7] F. K. Tittel, W. L. Wilson, R. E. Stickel, G. Marowsky, and W. E. Ernst, Appl. Phys. Lett. **36**, 405 (1980).
[8] F. K. Tittel, G. Marowsky, M. C. Smayling, and W. L. Wilson, Appl. Phys. Lett. **37**, 862 (1980).
[9] N. G. Basov, V. S. Zuev, A. V. Kanaev, L. D. Mikheev, and D. B. Shavroskii, Sov. J. Quantum Electron. **10**, 1561 (1980).
[10] M. Shahid, H. Jara, H. Pummer, H. Egger, and Ch. K. Rhodes, Opt. Lett. **10**, 448 (1985).
[11] N. Schwentner and V. A. Apkarian, Chem. Phys. Lett. **154**, 413 (1989); A. I. Katz, J. Feld, and V. A. Apkarian, Opt. Lett. **14**, 441 (1989).
[12] H. Kunttu, W. G. Lawrence, and V. A. Apkarian, J. Chem. Phys. (in press).
[13] H. P. Grieneisen, H. Xue-Jing, and K. L. Kompa, Chem. Phys. Lett. **82**, 421 (1981).
[14] G. Marowsky, R. Sauerbrey, F. K. Tittel, and W. L. Wilson Jr., Chem. Phys. Lett. **98**, 167 (1983).
[15] A. W. McCown and J. G. Eden, J. Chem. Phys. **81**, 2933 (1984).
[16] M. R. Berman, Chem. Phys. Lett. **157**, 562 (1989).
[17] E. Quinones, Y. C. Yu, D. W. Setser, and G. Lo, J. Chem. Phys. **93**, 333 (1990).
[18] L. Wiedeman, M. E. Fajardo, and V. A. Apkarian, J. Phys. Chem. **92**, 342 (1988).
[19] F. Okada, L. Wiedeman, and V. A. Apkarian, J. Phys. Chem. **93**, 127 (1989).
[20] W. G. Lawrence, F. Okada, and V. A. Apkarian, Chem. Phys. Lett. **150**, 339 (1988).
[21] A. I. Katz and V. A. Apkarian, J. Phys. Chem. **94**, 6671 (1990).
[22] *Thermophysical Properties of Neon, Argon, Krypton, and Xenon*, edited by V. A. Rabinovich, A. A. Vasserman, V. I. Nedostup, and L. S. Veksler, National Standard Reference Service of the USSR, Vol. 10 (Hemisphere, New York, 1988), p. 113.
[23] W. G. Lawrence and V. A. Apkarian, Israel J. Chem. **30**, 135 (1990).
[24] J. Le Calve, M. C. Castex, B. Jordan, G. Zimmerer, T. Moller, and D. Haaks, in *Photophysics and Photochemistry above 6 eV*, edited by F. Lahmani, (Elsevier, Amsterdam, 1985), p. 639.
[25] M. E. Fajardo and V. A. Apkarian, J. Chem. Phys. **85**, 5660 (1986).
[26] Y. C. Yu, D. W. Setser, and H. Horiguchi, J. Phys. Chem. **87**, 2209 (1983); J. K. Ku, G. Inoue, and D. W. Setser, *ibid.* **87**, 2989 (1983); D. W. Setser and J. K. Ku, in Ref. 24.
[27] H. Jara, H. Pummer, H. Egger, and Ch. K. Rhodes, Phys. Rev. B **30**, 1 (1984).
[28] V. A. Apkarian, Proceedings of International Conference on Lasers' 89, p. 121.
[29] M. C. Castex, J. Chem. Phys. **74**, 759 (1981).
[30] C. C. Kirkpatrick and L. A. Viehland, Chem. Phys. **98**, 221 (1985).
[31] J. O. Hirschfelder, C. F. Curtiss, and R. B. Bird, *Molecular Theory of Gases and Liquids* (Wiley, New York, 1954).

[32] A. Penner, A. Amirav, J. Jortner, and A. Nitzan, J. Chem. Phys. **93**, 147 (1990); N. Liver, A. Nitzan, A. Amirav, and J. Jortner, J. Chem. Phys. **88**, 3516 (1988).
[33] R. L. Fulton, J. Chem. Phys. **61**, 4141 (1974).
[34] B. Otto, J. Schroeder, and J. Troe, J. Chem. Phys. **81**, 202 (1984), and references therein.
[35] F. Okada, Masters thesis, UCI, Irvine, 1989.
[36] N. Schwentner and V. A. Apkarian (unpublished data).